

Numerical optimization of metasurface cells for acoustic reflection

Giorgio Palma^{*}, Francesco Centracchio[†], Lorenzo Burghignoli[‡], Ilaria Cioffi, and Umberto Iemma[§]
Roma Tre University, Via Vito Volterra, 62, 00146 Roma, RM, Italy

Metamaterials and metasurfaces disclosed new degrees of freedom in controlling the acoustic field. Exploiting the generalized Snell law and the generalized law of reflection, the assembly of subwavelength unit cells is able to achieve extraordinary refraction and reflection by means of controlled phase delay introduced in the field by the treated boundaries. The space-coiling design is one of the most powerful for cells in this metadevices class, providing effective low-thickness metasurfaces. However, space-coiling suffers from a narrow frequency operating range due to the intrinsic connection between the design operating wavelength and the characteristic dimensions of the metasurface. This work defines a procedure based on numerical optimization for designing space-coiling cells for modular acoustic metasurfaces extending the frequency range in which the metasurface is effective. The set comprises eight different unit cells, each introducing a tailored phase shift in the reflected field that can be arranged to produce the desired acoustic effect. The broadband design is obtained by minimizing the dependency on the operating frequency of phase delay introduced by the cells, keeping the overall thickness below a quarter of the design wavelength. Results are shown for the benchmark problem of a metasurface modifying the reflection angle from a boundary.

Nomenclature

- λ = wavelength of the acoustic perturbation
 λ_0 = nominal wavelength of the acoustic perturbation for cells' design
 f = frequency of the acoustic perturbation
 f_0 = nominal frequency of the acoustic perturbation corresponding to the nominal wavelength
 c = speed of sound
 N_c = number of cells composing the building set for metasurfaces

^{*}Post-Doc Research Fellow, Department of Civil, Computer Science and Aeronautical Technologies Engineering, giorgio.palma@uniroma3.it

[†]Research Fellow, Department of Civil, Computer Science and Aeronautical Technologies Engineering, francesco.centracchio@uniroma3.it

[‡]Research Assistant, Department of Civil, Computer Science and Aeronautical Technologies Engineering, lorenzo.burghignoli@uniroma3.it

[§]Full Professor, Department of Civil, Computer Science and Aeronautical Technologies Engineering, umberto.iemma@uniroma3.it

Presented as Paper AIAA 2019-2559 at the 25th AIAA/CEAS Aeroacoustics 2019 Conference, Delft, The Netherlands, June 20-23, 2019;

- k = cell index (from 1 to N_c)
- \mathbf{p} = acoustic pressure
- ϕ_i = acoustic phase of the incident acoustic perturbation at the cell-hosting domain interface
- ϕ_r = acoustic phase of the reflected acoustic perturbation at the cell-hosting domain interface
- $\Delta\phi$ = acoustic delay introduced by the cell at the cell-hosting domain interface defined as $\phi_r - \phi_i$
- θ_i = incident angle of acoustic perturbation on the metasurface interface
- θ_r = reflection angle of the acoustic perturbation from the metasurface interface
- R = complex-valued reflection coefficient
- J = objective function in the numerical optimization
- \mathbf{x} = variables vector in the numerical optimization, with components x_n
- \mathbf{y} = parameters vector in the numerical optimization, with components y_n
- g_i = inequality constraints in the numerical optimization
- h_j = equality constraints in the numerical optimization

I. Introduction

Several attempts to give a rigorous definition to the term metamaterial have been made since the end of the last century. Early interpretations were provided by researchers in the electromagnetic field, where metamaterials were investigated first, like Weiglhofer and Lakhtakia [1] or Cui et al. [2]. By combining their definitions, a metamaterial can be identified as a three-dimensional macroscopic composite of periodic or non-periodic structures able to produce responses not available in nature to a specific excitation by conventionally engineered materials. Metamaterials derive their properties from the designed structures and geometries more than from their chemical composition, and the behavior of properly defined unit cells can be translated into averaged effective parameters.

Starting from electromagnetism, the attention on metamaterials has rapidly spread into several research fields, such as acoustics and, more recently, aeroacoustics. Researchers in these fields proposed metamaterials showing peculiar properties, for example, negative effective bulk modulus and dynamic mass [3–6], negative refractive index [7–9] and anomalous high absorption or reflection coefficients at low frequencies overcoming the mass law [10–12]. Recently, Willis coupling, also known as bianisotropy in acoustics, has been proven and investigated [13, 14], opening the way to transfer effects enabled by bianisotropy from electrodynamics to acoustics.

An extensive review on metamaterials and their applications in acoustics is beyond the scope of this article, and the interested reader is referred to the numerous reviews available, for example, in Palma et al. [15], Yang and Sheng [16] and Cummer et al. [17].

To the aim of the present work, it is worth mentioning a specific class of acoustic metamaterials, the so-called

phase-gradient-based metamaterials. While most acoustic metamaterials exploit local resonances to produce their effects, the phase–gradient approach is based on structures, or cells, decorating some domain boundary, that can induce several peculiar behaviors through the introduction of a tailored distribution of phase delays in the reflected or refracted acoustic field [18, 19]. When a metamaterial device is built with a thickness significantly below the working wavelength, it is usually called a metasurface. Space-coiling metamaterials involving labyrinthine structures are inherently suitable for designing metasurfaces due to their feature of folding long channels multiple times to reduce the overall thickness. A reduced thickness is often desirable for a metamaterial as it widens the field of applicability in a broader range of real situations. There is, hence, a great interest in the research and development of metasurfaces. One of the most interesting designs that can be found in the literature presents metasurfaces engineered to show peculiar behaviours like arbitrarily-shaped virtual surfaces to modify the local reflection angle [18, 20, 21], or to obtain anomalous transmission for lens-like behaviours (see *e.g.* Xia et al. [22] where a dual layer metasurface is designed to achieve a one–way controlled transmission), or even to transform the propagation pattern from spherical to plane or surface waves [23, 24]. Recent advances have shown the possibility of exploiting the Willis coupling phenomenon to gain full control over the acoustic refraction, and avoid scattering towards undesired directions [14, 25].

A valuable study on an ultrathin metasurface can be found in Qi and Assouar [26], where a concept of a sub-wavelength reflective metasurface is numerically and analytically investigated: the results, obtained with 2D and 3D finite element analyses, validated the concept for acoustic focusing and energy confinement, showing the capability to be broadly applied in different fields of applications. Nonlocal passive metastructures have been studied by Quan and Alù [27] demonstrating, focusing on the canonical problem of beam steering, that such a design can mimic balanced gain and loss distributions, enabling unitary efficiency in wavefront transformation: to this aim, the authors introduced an interesting approach to realize low-profile planar metasurfaces using engineered nonlocality.

Recently, phase-gradient based metasurfaces have been explored as a new class of acoustic treatment for aeronautical applications. In Iemma and Palma [28], a metasurface with Helmholtz-resonator-based cells is used to create a shadow zone reducing the radiation from a 2D duct. Numerical simulations showed great potential in creating the so-called virtual scarfing of aero engine nacelles. The same problem is addressed in Palma and Burghignoli [29], using a metafluid model to optimize the phase-delay profile of the metasurface lining, and in Palma et al. [30] where the metafluid model is extended to account for curvatures of the geometry of a realistic nacelle. A wing lining for innovative blended-wing-body-like configurations with engines installed on top is imagined in Palma et al. [31] to enhance the acoustic shielding effect of the center section, using the same metafluid model and robust optimization.

Typically, the design of a metasurface for anomalous reflection/refraction is based on the choice of a nominal operating wavelength λ_0 that can be used as a basis for the definition of the constructive parameters of the surface itself, and the resulting effective bandwidth is typically narrow. So far, some authors have investigated the off-design performance of metadevices trying to obtain broadband effectiveness, also exploring different design strategies. Ding

et al. [32] addressed the problem of a narrow band transmission for refraction-controlling metasurfaces due to a significant impedance mismatch at the interface between air and metamaterial in space-coiling cells. To reduce this limitation, they added an impedance-matching section to helicoidal cells, effectively widening the transmission coefficient at the cost of an increased thickness. Wang et al. [33] included multi-order diffractions in the theoretical analysis of the modes reflected by phase-gradient metasurfaces. The proposed theory was exploited by the authors to design, fabricate and test a labyrinthine metasurface exhibiting anomalous behaviours such as negative reflection towards the direction of the incident wave, anomalous reflection below critical incidence and enhanced-absorption for higher order diffracted waves. In Dubois et al. [34] the authors investigated both numerically and experimentally the effect of the rapidly changing phase gradient on the cloaking performance of a deep-subwavelength metasurface formed by Helmholtz resonator. Ge et al. [35] numerically and experimentally demonstrated an open window structure composed of several blades lined with deep-subwavelength metasurfaces on both sides exhibiting either broadband unidirectional-acoustic-insulation and omnidirectional bidirectional-acoustic-insulation. Ghaffarivardavagh et al. [36] developed a space-coiling design with channels of varying height that are equivalent to a horn-like channel. The gradual change in channel height leads to the presence of an imaginary term in the acoustic impedance of the metasurface, which enables the possibility to simultaneously control both phase delay and amplitude of the reflected field with a passive device. The impedance matching is reached in Gong et al. [19] with a Helmholtz-resonator-based design for the metasurface cells. The phase shift of the cells is controlled by adjusting the width of the channel decorated with the resonators within a range in which the transmission coefficient is proven to be close to unity by numerical simulations.

Tian et al. [37] explored the use of pentamode metamaterials for modifying the local speed of sound, achieving remarkable results for underwater acoustic control. The use of the pentamode material reflects in a highly transmissive device, thanks to the inherent impedance matching with the hosting fluid, and in a frequency-independent metabehavior. However, the extension to pentamode materials for airborne sound would require density and bulk modulus properties inherently hard to be achieved. An interesting observation can be found in Zhu et al. [38], where it is pointed out that a non-dispersive relation is required between the frequency and the phase shift gradient provided by the metasurface in order to achieve broadband behavior. This linear relation is obtained, in the cited work, using elementary cells with straight channels as building blocks. To keep the broadband effectiveness of the metasurface, in addition, the authors do not build their devices using a predetermined set of elementary cells, and the maximum thickness of the device is not determined *a-priori*, but depends on the extension of the metasurface. Wu et al. [39] exploited the same design for underwater ultrasonic sound focusing. Even though this geometrical choice allows the designed phase shift gradient to remain unaltered for off-design frequencies, it necessarily yields a higher required thickness of the surface, at least half of the wavelength of the lowest frequency of interest. Wang et al. [40] used a spiral design for the space-coiling cells of a metasurface for acoustic carpet cloaking. The limited dispersion of this design ensures the skin cloak provides invisibility in a quite broad frequency range with a thickness not exceeding $1/7$ of the working wavelength.

The primary objective of the present work is to enhance the broadband performance of a metasurface designed for anomalous reflection, utilizing a set of space-coiling cells as building blocks and numerical optimization techniques. The objective is to retrieve the optimal values of the design variables of the cells of the set through numerical optimization, precisely aligning the phase shift induced by each cell and its frequency dynamics with a desired target. In this work, the target phase delay that the cells provide is required to be evenly spaced between 0 and 1.75π . In addition, numbering the cells of the set with the delay provided, the difference between the phase delay of two sequential cells is required to be as constant as possible with respect to operating frequency variations. Satisfying these requirements in a frequency band means increasing the bandwidth of any device built using the optimized cells as building blocks. The incorporation of space-coiling technology, in conjunction with optimization, allows us to address the inherent limitation of the device's bandwidth. Moreover, this approach enables us to leverage the benefits offered by the metasurface's reduced thickness, further enhancing its overall functionality.

The article is organized as follows. The design of a metasurface for anomalous acoustic reflection is described in Sec. II, followed by the formalization of the optimization process in Sec. III. Results of the numerical optimization are reported in Sec. IV, including the numerical assessment of the optimized metasurface through Finite Element Method (FEM) simulations.

II. Metasurface design

The design of a metasurface for anomalous acoustic reflection usually starts with the design of the N_c elementary cells to be used as bricks of the device. Each cell introduces a different phase shift $\Delta\phi = \phi_r - \phi_i$ in the acoustic reflected or transmitted field, in the range $0-2\pi$. The phase delay is hence referred to the phase of the incident field ϕ_i in correspondence with the interface between the metasurface and the exterior domain, *i.e.*, the phase of the wave reflected by a hard-wall in place of the metasurface. In other words, the phase delay is defined as the phase delay experienced by an acoustic wave reflected by the cell compared to a wave reflected by an acoustically hard wall. This approach is based on the generalized Snell's law for acoustic reflection and refraction [41], which stems from its analogous in optics [42]. Limiting our analysis to metasurfaces for extraordinary reflection and assuming the phase delay to vary in one spatial direction only, ξ , the reflection angle is given by:

$$\sin \theta_r = \frac{\lambda}{2\pi} \frac{\partial}{\partial \xi} \Delta\phi(\xi, \lambda) + \sin \theta_i, \quad (1)$$

where $\lambda = c/f$ is the wavelength of the incident wave, θ_i and θ_r are the incident and reflection angle, respectively, with respect to the normal to the metasurface-hosting domain interface plane. This equation links the extraordinary reflection behavior to the presence of a gradient of induced phase delay in the reflected wave by the metasurface; when there is no induced phase gradient at the interface, the relation between the incident and reflected wave is, as expected,

described by the traditional reflection law. Typically, the designer shall first identify the desired θ_r distribution along ξ , and hence the corresponding $\Delta\phi$ profile that the metasurface should induce in the reflected field, starting from the behaviour desired from the boundary where the metasurface will be employed, *e.g.*, mimicking a virtual inclination, inducing lens-like behaviours, diffusing the scattered field in all the directions, transforming the incident wave into surface waves, etc. Applying Eq. (1) for a given θ_r distribution along ξ , the designer will generally obtain $\Delta\phi(\xi)$ as a continuous function in space. However, only a piecewise approximation of the continuous $\Delta\phi$ profile is achievable by combining the elementary unit cells in the building set, since the cells have a finite width and a quantization error is unavoidable. By appropriately combining the elementary units, the designer would be able to build a metasurface introducing the desired phase-delay distribution in the reflected acoustic field and hence obtain the corresponding local extraordinary reflection angle [18, 20]. Fig. 2 summarizes schematically the above-mentioned steps for the design of a phase-gradient-based metasurface.

Figure 1 illustrates the parametrization of the generic unit cell adopted in the present work. It is entirely determined by the vector of the cell's geometry variables $\mathbf{x}_k = [n_w \ t \ a_x]^T$, where n_w , t , and a_x identify respectively the number of internal walls of the channel in the cell, the thickness of the lateral walls and the depth of the cell. The other geometrical quantities directly depend on this set or are constant parameters:

- $a_y = \lambda_0/8$ is the width of the cell.
- $w = 1 \text{ mm}$ is the thickness of the internal walls.
- $d = (a_x - w n_w)/n_w$ is the channel width.
- $l = a_y - d - 2t$ is the width of the internal walls.

Limiting the analysis to a monodimensional phase-delay gradient does not cause any lack of generality: a three-dimensional version of the cells used in the present work is easily obtained by adding a depth to the cells (for example equal to their width a_y), the phase-delay gradient along an orthogonal direction $\eta = \xi \times \zeta$ can be studied independently with the analogous of Eq. (1), and the cells arranged in a two-dimensional matrix to satisfy the designer's needs.

The choice of the value of the cell width a_y balances two needs. On one side, the width of the cell defines the maximum spatial resolution achievable in the piecewise approximation of $\Delta\phi(\xi, \lambda)$: the thinner the cell the better a rapidly changing phase delay profile from the continuous function can be followed by the metasurface approximation. On the other side, the acoustic channel in a very thin cell has less space to develop horizontally, and hence, for a given total length, the thickness of the cell needs to be increased, which is undesirable. The value $a_y = \lambda_0/8$ seems to be a good compromise and it has been mutated from Li et al. [20].

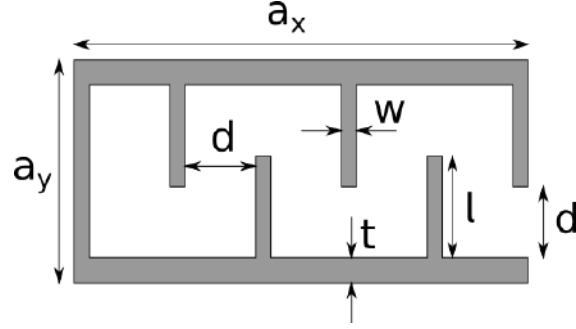


Fig. 1 Geometry of the parametrized unit cell ($n_w = 5$), with the graphical representation of its design variables and parameters: $w = 1$ mm, $a_y = \lambda_0/8$, $d = (a_x - w n_w)/n_w$, $l = a_y - d - 2t$.

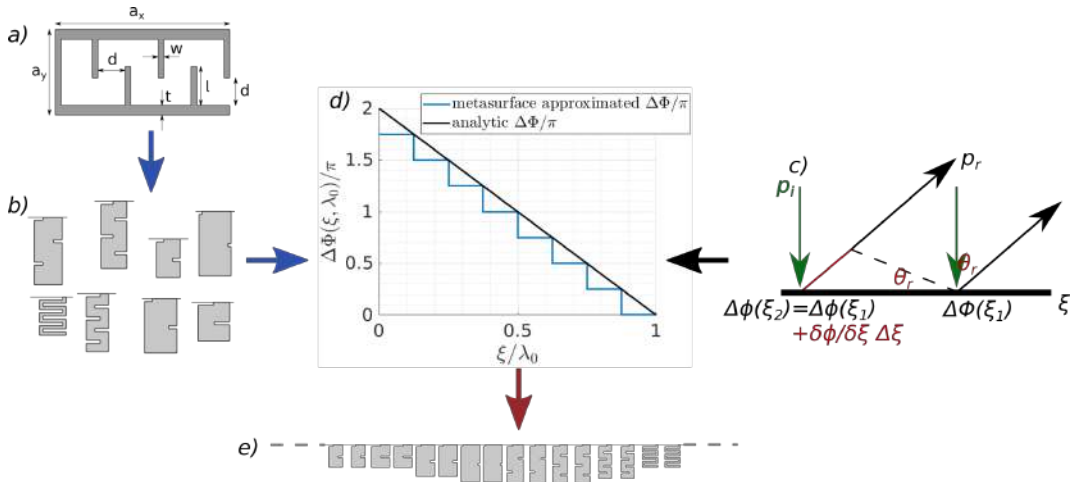


Fig. 2 Illustration of the steps for the design of a phase-gradient-based metasurface. First, the generic cell and its design variables are defined, a); then, the set of N_c cells composing the building set is created, each one able to introduce a tailored $\Delta\phi$ in the reflected field; the specific application defines the analytic profile of phase-delay required through Eq. (1), c); the cells in the building set define the stepwise approximation of the desired delay profile, d), and hence the arrangement of the cells building the metasurface, e).

The acoustic response of the elementary cells is obtained from direct linear lossless acoustic simulations using the commercial FEM solver Comsol Multiphysics, in terms of the argument of the complex reflection coefficient of the cell,

$$\Delta\phi(\mathbf{x}, \lambda) = \arg (R(\mathbf{x}, \lambda)) \quad (2)$$

In order to obtain an adequate resolution for the design of phase-delay profiles, the range $0-2\pi$ is divided into intervals of $\pi/4$. Therefore, the set of unit cells is composed of $N_c = 8$ different cells. The appropriate choice of the values of the components of \mathbf{x}_k for each of the cells allows the creation of a building set capable of satisfactorily approximating any $\Delta\phi$ profile as required from a specific application, when the cells are appropriately arranged in a metasurface. Naming the cells with ordinal numbers, for k from 1 to 8, the phase delays the cells are required to introduce in the reflected field for the nominal frequency are $0, \pi/4, \pi/2, 3\pi/4, \pi, 5/4\pi, 3/2\pi, 7/4\pi$, respectively. A set of reference non-optimized

cells is obtained in the present work for the nominal frequency $f_0 = 3430$ Hz, and hence $\lambda_0 = 0.1$ m. The geometries of the non-optimized reference cells have been defined arbitrarily fixing $a_x = \lambda_0/8$ for each of the eight cells and selecting a combination of values for t and n_w such that the phase delay of the cell was the one required. This is the common procedure also described in [18]. The values of the design variables for the non-optimized cells can be found in Tab. 1.

	#1	#2	#3	#4	#5	#6	#7	#8
n_w	6	5	4	3	2	2	2	2
t (mm)	1.4	3.5	2.06	1.67	1	1.02	1.08	2.42
a_x	$\frac{\lambda_0}{8}$	$\frac{\lambda_0}{5.291}$	$\frac{\lambda_0}{4.566}$	$\frac{\lambda_0}{4.566}$	$\frac{\lambda_0}{4.785}$	$\frac{\lambda_0}{5.650}$	$\frac{\lambda_0}{7.936}$	$\frac{\lambda_0}{8}$
$\frac{\Delta\phi(f_0)}{\pi}$	0	0.25	0.5	0.75	1	1.25	1.5	1.75

Table 1 Design variables values for the non-optimized eight cells and nominal phase delay provided.

For the specific application of a virtual inclined wall, which will be considered in Sec. IV, θ_r is a constant value along the metasurface boundary, and the required $\Delta\phi(\xi)$ profile obtained by Eq. (1) is a linear function proportional to λ . In this peculiar case, the metasurface is composed of a repeating sequence of elementary cells, which can be identified as the metasurface's unitary element. The metasurface analyzed in this work is characterized by $\theta_r = \pi/6$, with $\theta_i=0$, at the design frequency f_0 ; the repeating module is hence composed by the sequence of the eight cells of the building set, each one repeated twice. For the current virtually inclined wall application, the metasurface can be extended along ξ by exploiting this periodicity. The off-design behaviour of the metasurface, *i.e.*, for $f \neq f_0$, is critical. In general, each of the non-optimized cells experiences a different variation of the phase delay provided for a given change of the working frequency, and this can drift the $\Delta\phi(\xi)$ of the metasurface far away from the desired one. As mentioned in the introduction, an alternative approach is described by Zhu *et al.* in [38] which, however, is not resolute: even though the *dispersionless metasurface* described in their work can obtain remarkable results at off-design frequencies for small devices, the modularity of the metasurface is lost also for the virtually inclined wall application. In fact, their design necessarily uses straight-channeled cells to avoid the dependence of the phase-delay gradient along the metasurface from the operating frequency. However, in this way, the cells' thickness is not bounded and, for the virtually inclined wall, linearly grows with the extension of the metasurface, since a repeatable elementary block of cells is not present: forcibly identifying one would result in an undesired jump in the phase delay gradient arising at any conjunction of two metasurface "artificial periods". Our approach tries to overcome the issue of a phase-delay profile abruptly changing with working frequency, keeping the maximum thickness of the metasurface in the subwavelength range. Numerical optimization is adopted to find the best values for the cells' design variables that minimize the change in the metasurface delay profile in off-design conditions, keeping the difference among the phase delays introduced by the cells as constant as possible with respect to frequency. The phase delay gradient continuity between the last and the first cell of a

metasurface unit will be a fundamental requirement during the optimization of the cells in the present work, allowing to keep the modularity of the metasurface also at off-design conditions.

III. Definition of the optimization problem

The problem of the phase manipulation of acoustic waves by a metasurface is addressed through an optimization process, including in the merit function the desired metabehaviour of each elementary cell, to obtain their constructive parameters as a solution. As previously stated, one of the primary goals of this work to be reached through the optimization approach is improving the off-design behavior, *i.e.* the broadband effectiveness, of a space-coiling metasurface. This improvement can be reached if the distance between the cells in the phase delay space is kept almost constant when varying the operating frequency, *i.e.* in the ideal case $\left. \frac{\partial \Delta\phi(\lambda)}{\partial \lambda} \right|_k = \left. \frac{\partial \Delta\phi(\lambda)}{\partial \lambda} \right|_{k+1}$. In other words, all the cells should ideally experience the same change in the $\Delta\phi$ produced for $\lambda \neq \lambda_0$, or, again, the off-design behaviour of a metasurface can be improved if the difference between the phase delay provided by any two cells of the building set is not variable with the operating frequency.

A generic optimization problem consists in the search of the set of variables \mathbf{x} that yields to a minimum of the N_J objective functions $J_m(\mathbf{x}, \mathbf{y})$ while satisfying the $N_g + N_h$ constraints $g(\mathbf{x}, \mathbf{y})$ and $h(\mathbf{x}, \mathbf{y})$, and can be formalized as follows:

$$\begin{aligned}
 & \text{minimize/maximize } [J_1(\mathbf{x}, \mathbf{y}), \dots, J_m(\mathbf{x}, \mathbf{y}), \dots, J_{N_J}(\mathbf{x}, \mathbf{y})], & m = 1, \dots, N_J \text{ and } \mathbf{x} \in \mathcal{D}_{\mathbf{x}} \\
 & \text{with bounds } x_n^L \leq x_n \leq x_n^U, & n = 1, \dots, N_x \\
 & \text{subject to } g_i(\mathbf{x}, \mathbf{y}) \leq 0, & i = 1, \dots, N_g \\
 & \text{and } h_j(\mathbf{x}, \mathbf{y}) = 0, & j = 1, \dots, N_h
 \end{aligned} \tag{3}$$

where \mathbf{y} is the vector of the parameters, \mathbf{x} is the vector of the N_x design variables bounded by x_n^L and x_n^U in the design space $\mathcal{D}_{\mathbf{x}}$, $g_i(\mathbf{x})$ are the N_g inequality constraints and $h_j(\mathbf{x})$ are the N_h equality constraints. In the present application, $N_J = 1$ and \mathbf{x} represent the vector collecting the design variables vectors \mathbf{x}_c of each of the N_c cells to be optimized..

The objective function used in the present study considers the phase shift provided by each elementary cell within the considered frequency range, and their dynamics with respect to the frequency. The word dynamics is here intended as the desired function describing the variability of the delays with the frequency; in this work, for example, we tried to obtain cells with a delay that stays constant in frequency.). A fundamental requirement for the optimized set of cells is the capability to give a phase delay covering the full $0-2\pi$ range in order to be effectively combined to design the desired $\partial\Delta\phi/\partial\xi$. To reach the required phase delay $\overline{\Delta\phi}$ dynamics, it is necessary to correctly include the phase shift provided by each cell of the metasurface in the objective function. The cumulative difference between the current

and target phase delay for the cells, $\Delta\phi(\mathbf{x}, k, f)$ and $\overline{\Delta\phi}(k, f)$ respectively, has to be quantified and included into the optimization process: to this end, the distance δ_p between $\Delta\phi(\mathbf{x}, \xi, f)$ and $\overline{\Delta\phi}(\xi, f)$ in the L^p space can be defined in the cell-frequency domain $\mathcal{D} = [N_c \times [f_{min}, f_{max}]]$ as

$$\delta_p(\mathbf{x}) := \left[\frac{1}{N_c \Delta\xi \Delta f} \iint_{\mathcal{D}} \left| \Delta\phi(\mathbf{x}, k, f) - \overline{\Delta\phi}(k, f) \right|^p d\mathcal{D} \right]^{\frac{1}{p}} \quad (4)$$

being $\Delta f = f_{max} - f_{min}$ the analyzed frequency interval. Although the normalization with respect to the domain measure is not present in the standard definition of the L^p -norm, it does not modify the norm asymptotic behavior defined with Eq. (4). It is worth noting that as p increases, $\|\cdot\|_p$ tends to the maximum value of the argument of the norm. This property has a paramount relevance, as low values of p enhance the contribution of distributed differences. In contrast, high values of p emphasize local differences: such a behavior plays a key role in formalizing the objective function. The distance $\delta_p(\mathbf{x})$ defined above represents the objective of the minimization problem. The Euclidean distance (*i.e.* the L^2 norm) appears to be a good candidate to represent the difference between the actual phase shift and the target one in the domain \mathcal{D} since it guarantees an excellent detail of the distributed differences preserving a good representation of the point-wise objective properties. In the discrete domain, the objective function of the problem can be numerically evaluated as follows:

$$J(\mathbf{x}, \mathbf{y}) = \frac{1}{N_c \alpha_y (f_{max} - f_0)} \sqrt{\sum_{k=1}^{N_c} \sum_{j=1}^{N_f} \left[\Delta\phi(\mathbf{x}, k, f_j) - \overline{\Delta\phi}(k, f_j) \right]^2} \quad (5)$$

where $\mathbf{x} = [\mathbf{x}_1 \dots \mathbf{x}_{N_c}]^T$ is the design variables vector (see Tab. 2), collecting all the cells' geometrical variables, and \mathbf{y} is the vector of the parameters (fixed design parameters of the cells, ambient temperature and pressure, medium density, flow velocity, etc.).

Equation (4) holds regardless of the required phase delay dynamics for the cells and is general. The actual shape of $\overline{\Delta\phi}(k, f)$ and $\Delta\phi(\mathbf{x}, k, f)$ for the specific application addressed in the present work will be defined in Sec.IV.

Design Variable	Reference	Lower Bound	Upper Bound
a_x	$\lambda_0/8$	$\lambda_0/16$	$\lambda_0/4$
n_w	5	2	6
t (mm)	1	1	t_{max}

Table 2 Design variables of each cell: reference value, lower bound and upper bound.

It is worth noting that the value of t_{max} in Tab. 2) is dependent on a_x and n_w to ensure the consistency of the constructive parameters, and its value can be assessed by evaluating an inequality constraint as it follows:

$$g_1(\mathbf{x}) = 2t - a_y + d < 0 \quad (6)$$

A pseudo-objective function has been defined using a quadratic penalty function to avoid the constraints' direct management. The minimization is achieved through a Particle Swarm Optimization (PSO) algorithm, originally introduced by Kennedy and Eberhart [43]. PSO is based on the social-behavior metaphor of a flock of birds or a swarm of bees searching for food and belongs to the class of heuristic algorithms for evolutionary derivative-free global optimization. The PSO scheme used here is an original deterministic implementation (DPSO) introduced by the Resistance & Optimization team of CNR-INM, the Institute of Marine Engineering of the Italian Research Council (the interested reader can find useful details in Campana et al. [44, 45]). The update at iteration $n + 1$ of the design point \mathbf{x}_i identified by the i^{th} individual of the swarm is given by

$$\mathbf{v}_i^{n+1} = \chi [\mathbf{v}_i^n + c_1 (\mathbf{p}_i - \mathbf{x}_i^n) + c_2 (\mathbf{g} - \mathbf{x}_i^n)] \quad (7)$$

$$\mathbf{x}_i^{n+1} = \mathbf{x}_i^n + \mathbf{v}_i^{n+1} \quad (8)$$

where χ is a constriction factor, c_1 and c_2 are the the social and cognitive learning rate, and \mathbf{p}_i and \mathbf{g} are the personal and global best, respectively. Systematic studies on both the formulation and the performance of DPSO can be found in Serani et al. [46], Pellegrini et al. [47], with the definition of suitable guidelines for Simulation-Based Design Optimization (SBDO) applied to ship design. Moreover, an initial efficiency comparison between the multiobjective DPSO and the genetic algorithm has been performed in Iemma et al. [48] for aeronautical problems.

IV. Numerical results

In the present work, the actual shape of $\overline{\Delta\phi}(\xi, f)$ is obtained by the considerations made at the beginning of Sec.III: ideally, each cell of the optimized set should exhibit the same variation of the phase delay introduced in the reflected field for a given variation of the operating frequency. The objective function in Eq.(5) is built using $N_f = 9$ frequencies equally spaced in the range 3230 – 3630 Hz and, for each frequency, the target phase delay of the i -th cell is defined such that

$$\begin{aligned} \overline{\Delta\phi}(k+1, f_j) - \overline{\Delta\phi}(k, f) &= \frac{\pi}{4} \quad \text{and} \\ \overline{\Delta\phi}(1, f_j) + 2\pi - \overline{\Delta\phi}(N_c, f) &= \frac{\pi}{4} \quad \text{with } 0 \leq \overline{\Delta\phi} \leq 2\pi \end{aligned} \quad (9)$$

The latter condition is introduced to drive the optimization towards a set of cells that guarantee the modularity of a metasurface built using them. The optimization analysis is performed with the optimization framework integrated inside the MDO tool FRIDA (FRamework for Integrated Design of Aircraft), suitably adapted to the present analysis. The minimization problem is then solved with a fixed budget of 72.000 objective function evaluations, using 72 particles and setting the maximum number of iterations to 1000. Figure 3 shows the convergence history of the process. Less than 10.000 objective function evaluations are needed for the optimization algorithm to reach a substantial convergence, with a reduction of the objective function value of 70% of its starting value.

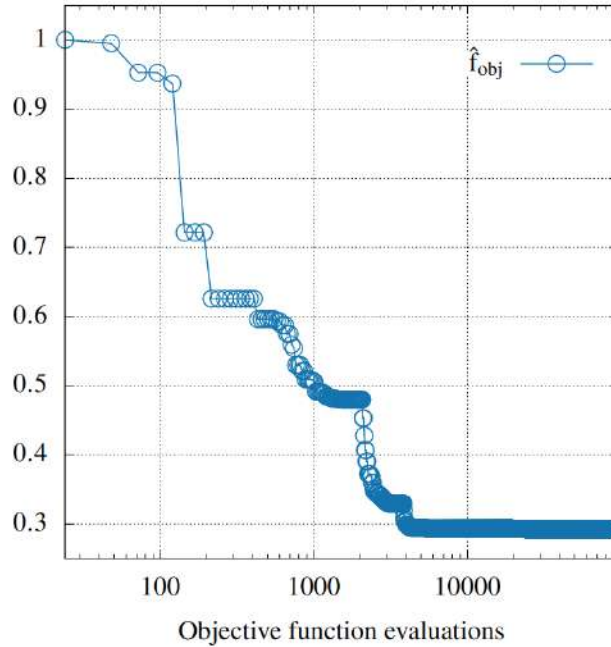


Fig. 3 Convergence trend of the objective function during the optimization process.

As a benchmark case, two metasurfaces have been built to steer the reflected field acting like an inclined wall,

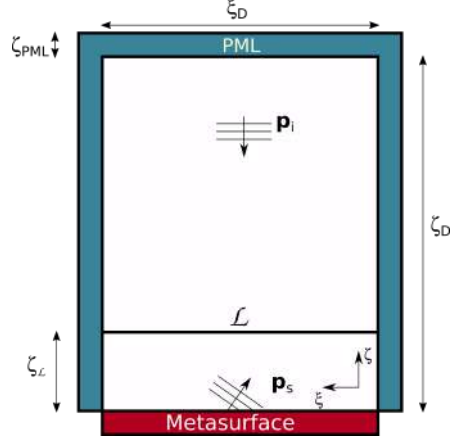


Fig. 4 Sketch of the computational domain for FEM simulations of extraordinary reflection from metasurfaces.

one using a set of non-optimized cells and one using the optimized set. The $\partial\Delta\phi(\mathbf{x}, \xi, \lambda)/\partial\xi$ is designed to obtain a reflection angle $\theta_r = \pi/6$ with $\theta_i=0$ and $\lambda_0 = 0.1$ m ($f_0 = 3430$ Hz) according to Eq.1. The acoustic performances of the two metasurfaces are then simulated using a linear acoustics model. The two-dimensional computational domain sketched in Fig. 4 consists of a rectangular area of sides $\xi_D = 12\lambda_0$, $\zeta_D = 20\lambda_0$ with the metasurface interfacing at one side. The Helmholtz equation is solved in the whole domain (cells and rectangle) for monochromatic periodic pressure perturbations

$$\frac{\omega^2}{c^2}\tilde{p} + \nabla\tilde{p} = 0 \quad (10)$$

with c and ω being the speed of sound and the angular frequency of the acoustic waves, respectively, and \tilde{p} is the complex-valued amplitude of the Fourier-transformed acoustic pressure at the frequency f . Eq. (10) is completed by the plane wave radiative boundary conditions imposed at the side of the rectangle opposed to the metasurface (producing a plane wave normally impinging on the metasurface interface as incident acoustic field) and a set of perfectly matched layers of thickness $\zeta_{\text{PML}} = 10\lambda_0$ surrounding three sides of the rectangle (the one with the metasurface is excluded) to truncate the computational domain without undesired reflection from the boundaries. Equation (10) is recast in his weak formulation and solved using the FEM using the commercial solver Comsol Multiphysics.

The non-optimized metasurface is able to guarantee the desired extraordinary reflection in a neighborhood of the design frequency. However, as can be seen from Fig. 5, the performance of the metasurface rapidly deteriorates at slightly lower or higher frequencies. At 3080Hz, the reflected field is spread in the domain, with several directivity lobes visible in Sec. IV; at 3680Hz, the wavefronts of the reflected wave are distorted and no longer planar, and some reflections towards undesired directions can also be noted in Sec. IV.

The value of the design variables of the cells obtained with the optimization procedure are reported in Tab. 3. The building cells composing the optimized metasurface have their range of operating frequencies extended through the single-objective optimization previously described, which reflects in a larger effective bandwidth of the metasurface

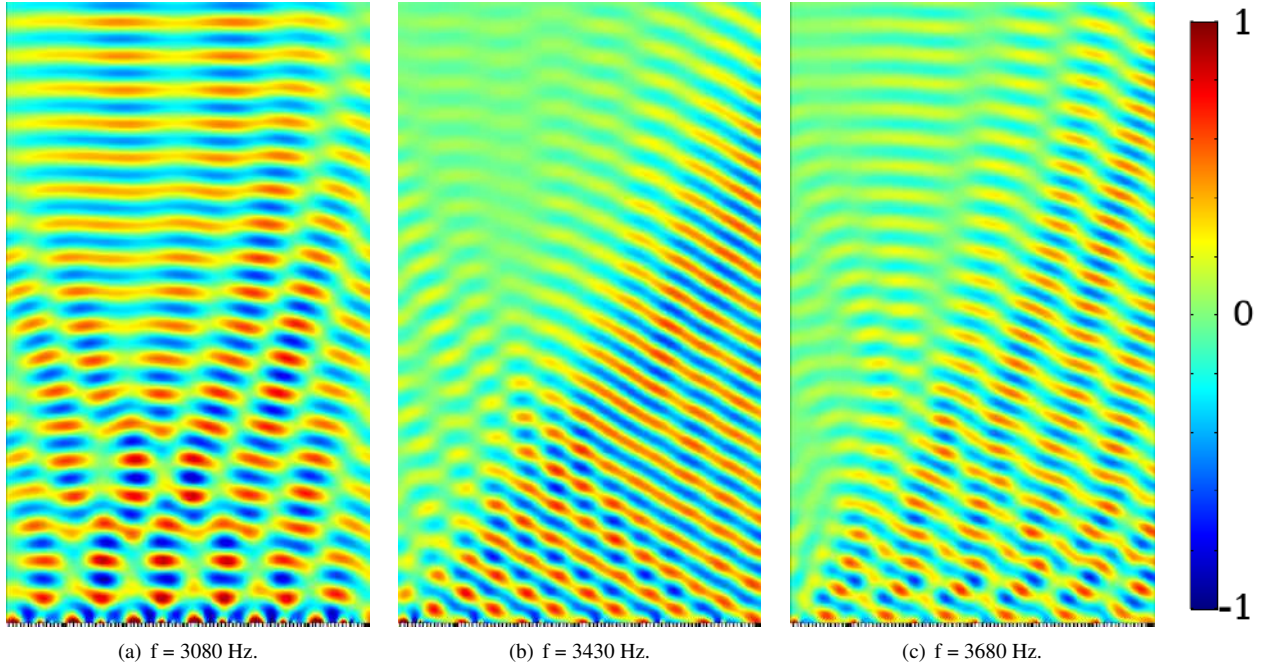


Fig. 5 Real part of the pressure field normalized with its maximum value in the domain hosting the metasurface scattered from the non-optimized metasurface when impinged by a plane wave incoming from the upper side at different frequencies.

created with those.

The reflected pressure fields from the optimized metasurface are shown in Fig.6 for the design frequency f_0 and the same two off-design frequencies of Fig. 5, exhibiting effective steering even though with slightly different angles. This change in the reflection angle is expected from Eq.1 as the optimized cells aimed at a $\partial\Delta\phi/\partial\xi$ constant in frequency. The spurious reflections at 3080 Hz, that were noted in Sec. IV for the reference metasurface, have been considerably reduced with the optimal cells. The reflection control performances have been improved also at 3680 Hz as the wavefronts of the reflected wave appear almost planar as desired.

To better compare the performance of the reference and the optimized solutions, the absolute value of the acoustic pressure is evaluated over a reference line \mathcal{L} parallel to the interface between the external domain and the metasurface, at a distance of $10\lambda_0$ from the latter for the octave band centered on the design frequency, see Fig. 9. The line \mathcal{L} is represented in the figure on the y-axis with its normalized length from 0 to 1, corresponding to the right and left extremities, respectively, of the line in Fig. 5 and Fig. 6. Figure 9 clearly shows that the optimization widened the effective frequency band of the metasurface: when the extraordinary reflection is happening, the scattered acoustic pressure is focused in the lower part of the picture (that corresponds to the right-hand side of \mathcal{L} in Figs. 5 and 6), as the incoming wave is reflected predominantly with the desired angle $\theta_r = \pi/6$. On the contrary, the shadowed bands in the pictures represent the ineffective frequency ranges, in which the reflection is spread towards multiple

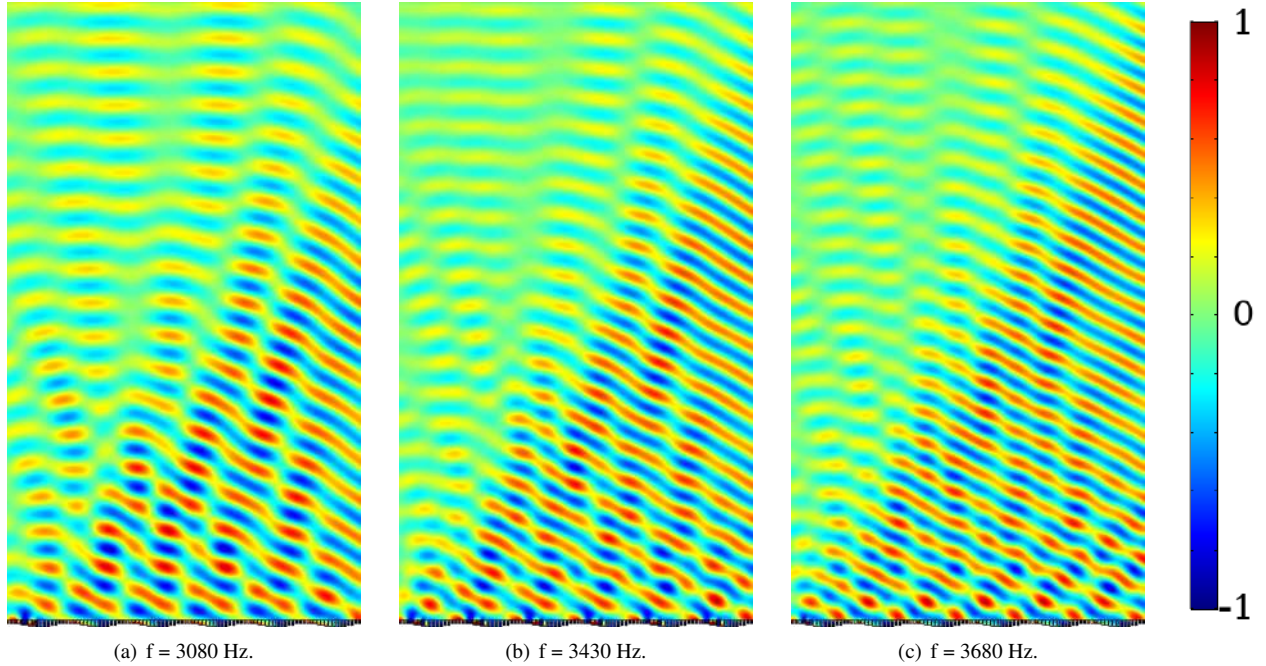


Fig. 6 Real part of the pressure field normalized with its maximum value in the domain hosting the metasurface scattered from the optimized metasurface when impinged by a plane wave incoming from the upper side at different frequencies.

directions. The presence at some frequency of red spots in the upper half of the maps in Fig. 9 means, in fact, that the metasurface is not steering the reflected wave properly for the corresponding frequency, since the reflected field is spread on the whole line and not only in the lower half as expected. This result is confirmed by directly comparing the field scattered by reference and optimized metasurfaces at various frequencies, depicted in Figure 10 : the non-optimized cells succeed in obtaining the required $\theta_r = \pi/6$ only at the design frequency, as shown in Fig. 10(f) where the reflected acoustic waves are directed in the desired direction with neat wavefronts. At the other analyzed frequencies, the scattering of the reflected acoustic waves towards undesired directions is clearly visible for the non-optimized case, Fig. 10(a), Fig. 10(d), Fig. 10(j), Fig. 10(m). The optimized cells, on the contrary, strongly reduce the performance decay outside the design frequency as shown in Fig. 10(c), Fig. 10(f), Fig. 10(i), Fig. 10(l), and 10(o), where the reflected field is orderly directed in the required direction.

The optimizer effectively selected the design parameters for the eight cells, such that the phase delay distance between consecutive cells has a small variation with frequency. This broadened the bandwidth of a benchmark metasurface to a 600 Hz-wide frequency range centered on the design frequency of the reference metasurface, between 3080 and 3680 Hz. Some optimal cells also show a negligible variation of their delay response in the considered frequency range, while others exhibit some difference in the delay provided in off-design conditions compared to the design frequency. The difference in the frequency dynamics of the delays of the various cells is responsible for the imperfections in the

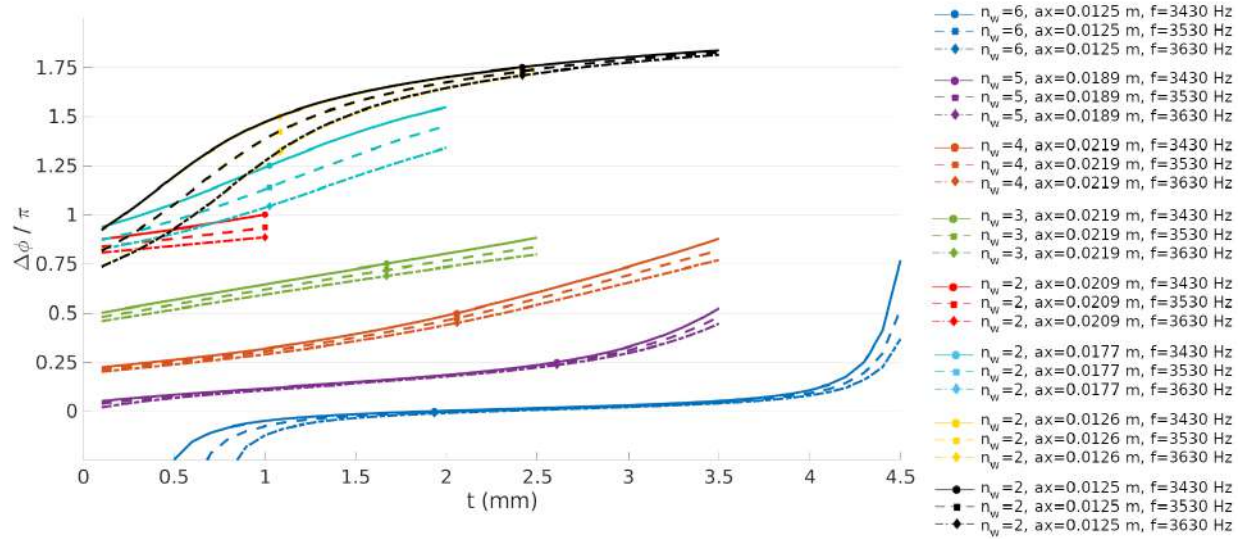


Fig. 7 $\Delta\phi/\pi$ for the optimized cells as a function of t for the optimal n_w and a_x . Three curves are plotted for each cell (grouped by color) representing the behaviour at 3430 Hz (solid), 3530 Hz (dashed), and 3630 Hz (dash-dotted). The optimal values for t for each cell are marked by dots, squares, and diamonds at 3430 Hz, 3530 Hz, and 3630 Hz respectively.

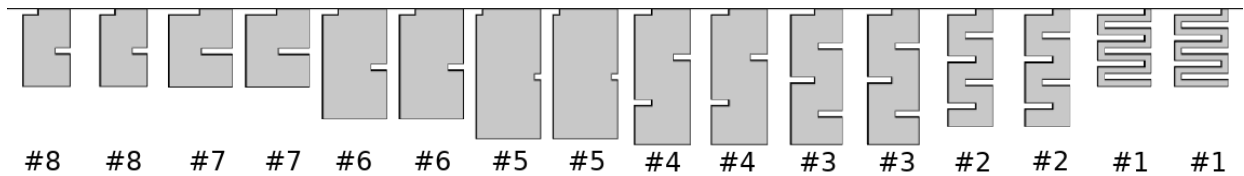


Fig. 8 Design of the optimal cells arranged in a metasurface for acoustic steering, $\theta_r(\lambda_0) = \pi/6$. The cells are numbered increasingly with the phase delay provided.

	#1	#2	#3	#4	#5	#6	#7	#8
n_w	6	5	4	3	2	2	2	2
t (mm)	1.93	2.61	2.06	1.67	1	1.02	1.08	2.42
a_x	$\frac{\lambda_0}{8}$	$\frac{\lambda_0}{5.291}$	$\frac{\lambda_0}{4.566}$	$\frac{\lambda_0}{4.566}$	$\frac{\lambda_0}{4.785}$	$\frac{\lambda_0}{5.650}$	$\frac{\lambda_0}{7.936}$	$\frac{\lambda_0}{8}$
$\frac{\Delta\phi(f_0)}{\pi}$	0	0.25	0.5	0.75	1	1.25	1.5	1.75

Table 3 Design variables values for the optimized eight cells and nominal phase delay provided.

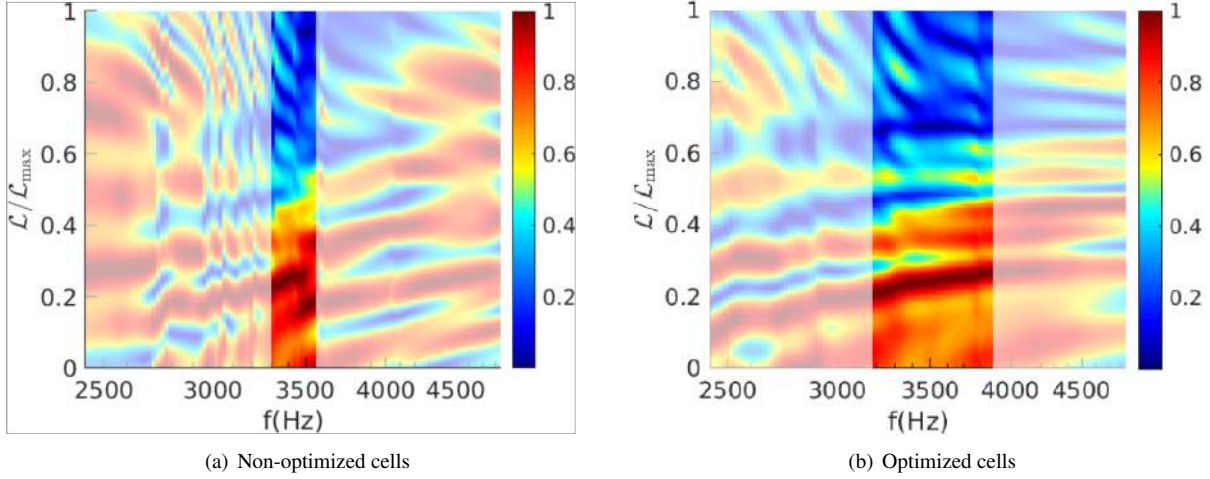


Fig. 9 Absolute value of the reflected acoustic pressure field divided by its maximum at line \mathcal{L} distant $\zeta_{\mathcal{L}} = 10\lambda_0$ from the metasurface interface.

reflection control that can still be noted for the optimized metasurface. The most critical cell is the one providing $\Delta\phi(f_0)/\pi = 1.25$, which has the less tortuous internal channel (note that a straight channel would have a linear relation between the operating frequency and the phase delay provided for a given length). This choice is somehow forced for the optimizer to reach the required delay for the mentioned cell. As a consequence, the cells providing $\Delta\phi(f_0)/\pi = 1$ and 1.5 are also characterized by a significant, yet smaller, variation of the delay with respect to frequency, that minimizes as much as possible the objective function as expressed in Eq. (5) and Eq. (9). The optimizer is limited in its struggle to find the ideal solution by the limited extension of the design domain and codomain. The results may be improved by enlarging the design space acting on the base design of the cells: one may try to change the cell type or mix different ones, including concepts such as Helmholtz resonators, perforated panels, topologically optimized cells, etc., in the available set of parametrized geometries aside of the spacecoiling cells, looking for the most suitable combination to keep the delay distance between the cells as constant as possible in frequency. The operative frequency band of the optimized metasurface has been effectively extended in a range comparable to the one considered in the objective function with N_f . However, the desired performances are not ensured outside of that bound nor to be reached in the

entire frequency range in the case an extremely large frequency interval is required. The method should be seen as a way to extend the operation bandwidth of metasurfaces based on dispersive cells that are typically needed for subwavelength designs through a smart selection of the design parameters. However, the success of the operation is obviously bonded with the domain and codomain extension.

Visco-thermal losses can play an important role in the acoustics of the structures studied in the present work. This is particularly true for cells with narrow channels possibly folded multiple times (*i.e.*, with a long equivalent length). In the present article, losses have been neglected in the derivation of the optimal cells. The very same cells have been analyzed considering their lossy behavior in Palma and Iemma [49]; it is shown that, in the specific case of the cells resulting from the optimization, losses play a significant role in cells #1, #2, and #3, due to their thin channels. However, considering $l_{eq} = n_w \sqrt{(w+d)^2 + (l+d)^2}$ as a rough estimation of the equivalent lengths of their folded channel, as suggested in [36], it is found that the quarter-wavelength resonant frequencies of the mentioned cells lie outside of the design frequency range. Some simulations are performed, including the effect of visco-thermal losses through an equivalent complex-valued speed of sound obtained from Pierce's model[50],

$$\frac{\omega}{c_{lossy}} = \frac{\omega}{c} + (1-i)a_{walls}, \quad \text{with} \quad a_{walls} = \frac{1}{cd_{eq}} \sqrt{\frac{\omega\eta}{2\rho_0}} \left(1 + \frac{\gamma-1}{\sqrt{Pr}} \right) \quad (11)$$

where d_{eq} is an equivalent hydraulic diameter of the channel set as d of the cell, γ is the ratio of the specific heats, and Pr is the Prandtl number. Eq. (11) has also been applied in Palma and Iemma [49] where the approach has been validated against full thermoviscous simulations of the cells. The results in Fig. 11 show that the wavefront manipulation performances of the metasurface are not compromised by including the losses in the optimized cells, with minor modifications in the effectiveness frequency range as extended by the optimization. Fig. 12 evidences a substantial change in the behavior of the metasurface outside of the frequency bounds considered in the optimization compared to Fig. 9(b), in particular for $f < 2500\text{Hz}$ and around $f \approx 4500\text{Hz}$, where sort of discontinuities in the reflection pattern appear. The quarter-wavelength resonant frequencies of the first three cells lie in the first frequency range, while the second value roughly corresponds to the second resonant frequency of the cell #1 (consider that the evaluation of the equivalent length is a rough approximation, see Palma and Iemma [49]).

In principle, the extraordinary reflection from the metasurface can be affected by the different grades of loss characterizing the different cells composing the device for a given frequency: the metabehaviours rely on the constructive and destructive interaction of the reflected waves by the cells, which can be strongly modified when the sound absorption of the various cells are very different one from the other, even when the phase delay profile of the metasurface perfectly follows the theoretically required one. The effect of visco-thermal losses may be included in the derivation of the optimal design of the cells; a possible strategy would be the introduction of an additional objective in the optimization, preferring cells with a similar real part in their normal incidence absorption (or equivalently, reflection) coefficients for

the frequencies of interest. A homogeneous level of losses between the cells implies that the metasurface would still modify the reflected wavefront as in the lossless case, but the amplitude of the reflected field would be attenuated. This behavior may or may not be acceptable depending on the specific application. In the latter case, the real part of the absorption coefficient should also be minimized as an additional objective.

V. Conclusions

The paper presents an approach based on numerical optimization for designing cells for acoustic metasurfaces dedicated to extraordinary reflection. Metasurfaces exploiting the generalized reflection law are often built using cells with a subwavelength thickness showing a dispersive relation between the phase delay and the operating frequency, leading, however, to devices typically characterized by a narrowband operational range with rapidly decaying performance in off-design conditions. In this work, the continuous domain of the acoustic delays is quantized with eight equispaced values between 0 and 2π ; each value is then assigned to one of the eight elementary cells composing the building set for generic metasurfaces for reflection control. Several combinations of the design variables of a suitably parameterized unit cell can be found such that it can provide a given phase delay in the reflected acoustic field. Numerical optimization can, hence, be used to explore the design domain, looking for the optimal set of variables of the optimal building set to broaden the operating frequency range of the metasurfaces. This is achieved by minimizing an objective function describing the difference in the frequency-related variation of the phase delays between the cells of the building set, which is a particular case of matching the phase-delay frequency dynamics for each cell to a suitably defined target. The optimized cells have been arranged to design a flat metasurface emulating the reflected acoustic field from an inclined wall. The optimization approach has been demonstrated to effectively broaden the response of the benchmark metasurface to a 600 Hz-wide frequency range centered on the design frequency of the reference metasurface. The process can be interpreted as an improvement of the robustness of the design with respect to the single-frequency design, making the resulting device capable of a broadband response not achievable by the reference design. The presented analysis has been conducted neglecting the visco-thermal effects occurring in the acoustic boundary layer. The performances of the metasurface built with the optimal cells have been afterward tested including the acoustic losses in the FEM simulations. The results showed little change in the reflection properties of the metasurface in the effective frequency band. The major differences instead arise at the frequencies corresponding to the resonance of the cells exhibiting the highest level of losses, outside of the operating frequency band of the metasurface. However, thermoviscous losses can generally play a significant role in determining the performance of the metasurfaces, and a way to effectively include them from the beginning of the design process as additional objective functions in the optimization has been proposed. In principle, the method is extensible to other required frequency dynamics of the phase delays provided by the elementary cells. However, the achievable results are mainly controlled by the extension of the optimization codomain, which is deeply connected to the respective domain, *i.e.* the specific design of the cell

used as parameterized elementary unit. The proposed method can be easily extended to enrich the space of the feasible solutions (*i.e.*, the optimization codomain), by including multiple parameterized concepts in the set of unit cells available to the optimization process (*i.e.*, the optimization domain).

References

- [1] Weiglhofer, W. S., and Lakhtakia, A., *Introduction to Complex Mediums for Optics and Electromagnetics*, SPIE—The International Society for Optical Engineering, P.O. Box 10 Bellingham, Washington 98227-0010 USA, 1999.
- [2] Cui, T. J., Liu, R., and Smith, D. R., *Introduction to Metamaterials*, Springer US, Boston, MA, 2010, Chap. 1, pp. 1–19. https://doi.org/10.1007/978-1-4419-0573-4_1, URL https://doi.org/10.1007/978-1-4419-0573-4_1.
- [3] Li, J., and Chan, C. T., “Double-negative acoustic metamaterial,” *Phys. Rev. E*, Vol. 70, 2004, p. 055602. <https://doi.org/10.1103/PhysRevE.70.055602>, URL <https://link.aps.org/doi/10.1103/PhysRevE.70.055602>.
- [4] Ding, Y., Liu, Z., Qiu, C., and Shi, J., “Metamaterial with Simultaneously Negative Bulk Modulus and Mass Density,” *Phys. Rev. Lett.*, Vol. 99, 2007, p. 093904. <https://doi.org/10.1103/PhysRevLett.99.093904>, URL <https://link.aps.org/doi/10.1103/PhysRevLett.99.093904>.
- [5] Liu, X. N., Hu, G. K., Huang, G. L., and Sun, C. T., “An elastic metamaterial with simultaneously negative mass density and bulk modulus,” *Applied Physics Letters*, Vol. 98, No. 25, 2011, p. 251907. <https://doi.org/10.1063/1.3597651>.
- [6] Cselyuska, N., Sečujski, M., and Crnojević-Bengin, V., “Novel negative mass density resonant metamaterial unit cell,” *Physics Letters A*, Vol. 379, No. 1, 2015, pp. 33 – 36. <https://doi.org/https://doi.org/10.1016/j.physleta.2014.10.036>, URL <http://www.sciencedirect.com/science/article/pii/S0375960114010858>.
- [7] Pendry, J. B., “Negative refraction makes a perfect lens,” *Physical review letters*, Vol. 85, No. 18, 2000, p. 3966.
- [8] Liu, Z., Zhang, X., Mao, Y., Zhu, Y. Y., Yang, Z., Chan, C. T., and Sheng, P., “Locally Resonant Sonic Materials,” *Science*, Vol. 289, No. 5485, 2000, pp. 1734–1736. <https://doi.org/10.1126/science.289.5485.1734>, URL <http://science.sciencemag.org/content/289/5485/1734>.
- [9] Brunet, T., Merlin, A., Mascaro, B., Zimny, K., Leng, J., Poncelet, O., Aristégui, C., and Mondain-Monval, O., “Soft 3D acoustic metamaterial with negative index,” *Nature Materials*, Vol. 14, 2014, p. 384. <https://doi.org/10.1038/nmat4164>, URL <http://dx.doi.org/10.1038/nmat4164>.
- [10] Sui, N., Yan, X., Huang, T.-Y., Xu, J., Yuan, F.-G., and Jing, Y., “A lightweight yet sound-proof honeycomb acoustic metamaterial,” *Applied Physics Letters*, Vol. 106, No. 17, 2015, p. 171905. <https://doi.org/10.1063/1.4919235>, URL <https://doi.org/10.1063/1.4919235>.
- [11] Gao, N., and Hou, H., “Low frequency acoustic properties of a honeycomb-silicone rubber acoustic metamaterial,” *Modern Physics Letters B*, Vol. 31, No. 11, 2017, p. 1750118. <https://doi.org/10.1142/S0217984917501184>.

- [12] Starkey, T. A., Smith, J. D., Hibbins, A. P., Sambles, J. R., and Rance, H. J., “Thin structured rigid body for acoustic absorption,” *Applied Physics Letters*, Vol. 110, No. 4, 2017, p. 041902. <https://doi.org/10.1063/1.4974487>, URL <https://doi.org/10.1063/1.4974487>.
- [13] Sieck, C. F., Alù, A., and Haberman, M. R., “Origins of Willis coupling and acoustic bianisotropy in acoustic metamaterials through source-driven homogenization,” *Phys. Rev. B*, Vol. 96, 2017, p. 104303. <https://doi.org/10.1103/PhysRevB.96.104303>, URL <https://link.aps.org/doi/10.1103/PhysRevB.96.104303>.
- [14] Quan, L., Ra’di, Y., Sounas, D. L., and Alù, A., “Maximum Willis Coupling in Acoustic Scatterers,” *Phys. Rev. Lett.*, Vol. 120, 2018, p. 254301. <https://doi.org/10.1103/PhysRevLett.120.254301>, URL <https://link.aps.org/doi/10.1103/PhysRevLett.120.254301>.
- [15] Palma, G., Mao, H., Burghignoli, L., Göransson, P., and Iemma, U., “Acoustic Metamaterials in Aeronautics,” *Applied Sciences*, Vol. 8, No. 6, 2018. <https://doi.org/10.3390/app8060971>, URL <http://www.mdpi.com/2076-3417/8/6/971>.
- [16] Yang, M., and Sheng, P., “Sound Absorption Structures: From Porous Media to Acoustic Metamaterials,” *Annual Review of Materials Research*, Vol. 47, No. 1, 2017, pp. 83–114. <https://doi.org/10.1146/annurev-matsci-070616-124032>, URL <https://doi.org/10.1146/annurev-matsci-070616-124032>.
- [17] Cummer, S. A., Christensen, J., and Alù, A., “Controlling sound with acoustic metamaterials,” *Nature Reviews Materials*, Vol. 1, No. 3, 2016, p. 16001.
- [18] Li, Y., Liang, B., Gu, Z.-m., Zou, X.-y., and Cheng, J.-c., “Reflected wavefront manipulation based on ultrathin planar acoustic metasurfaces,” *Scientific Reports*, Vol. 3, 2013, p. 2546. <https://doi.org/10.1038/srep02546>.
- [19] Gong, K., Wang, X., Ouyang, H., and Mo, J., “Tuneable gradient Helmholtz-resonator-based acoustic metasurface for acoustic focusing,” *Journal of Physics D: Applied Physics*, Vol. 52, No. 38, 2019, p. 385303. <https://doi.org/10.1088/1361-6463/ab2b85>, URL <https://doi.org/10.1088/1361-6463/ab2b85>.
- [20] Li, Y., Jiang, X., Li, R.-q., Liang, B., Zou, X.-y., Yin, L.-l., and Cheng, J.-c., “Experimental Realization of Full Control of Reflected Waves with Subwavelength Acoustic Metasurfaces,” *Phys. Rev. Applied*, Vol. 2, 2014, p. 064002. <https://doi.org/10.1103/PhysRevApplied.2.064002>, URL <https://link.aps.org/doi/10.1103/PhysRevApplied.2.064002>.
- [21] Chen, H., “Anomalous Reflection of Acoustic Waves in Air with Metasurfaces at Low Frequency,” *Advances in Condensed Matter Physics*, Vol. 2018, 2018.
- [22] Xia, J.-p., Zhang, X.-t., Sun, H.-x., Yuan, S.-q., Qian, J., and Ge, Y., “Broadband Tunable Acoustic Asymmetric Focusing Lens from Dual-Layer Metasurfaces,” *Physical Review Applied*, Vol. 10, No. 1, 2018, p. 014016. <https://doi.org/https://doi.org/10.1103/PhysRevApplied.10.014016>.
- [23] Wang, W., Xie, Y., Konneker, A., Popa, B.-I., and Cummer, S. A., “Design and demonstration of broadband thin planar diffractive acoustic lenses,” *Applied Physics Letters*, Vol. 105, No. 10, 2014, p. 101904. <https://doi.org/10.1063/1.4895619>, URL <https://doi.org/10.1063/1.4895619>.

- [24] Xie, Y., Wang, W., Chen, H., Konneker, A., Popa, B.-I., and Cummer, S. A., “Wavefront modulation and subwavelength diffractive acoustics with an acoustic metasurface,” *Nature Communication*, Vol. 5, 2014, p. 5553. <https://doi.org/10.1038/ncomms6553>.
- [25] Li, J., Shen, C., Díaz-Rubio, A., Tretyakov, S. A., and Cummer, S. A., “Systematic design and experimental demonstration of bianisotropic metasurfaces for scattering-free manipulation of acoustic wavefronts,” *Nature Communications*, Vol. 9, No. 1, 2018, p. 1342. <https://doi.org/10.1038/s41467-018-03778-9>, URL <https://doi.org/10.1038/s41467-018-03778-9>.
- [26] Qi, S., and Assouar, B., “Ultrathin acoustic metasurfaces for reflective wave focusing,” *Journal of Applied Physics*, Vol. 123, No. 23, 2018, p. 234501. <https://doi.org/10.1063/1.5031482>.
- [27] Quan, L., and Alù, A., “Passive Acoustic Metasurface with Unitary Reflection Based on Nonlocality,” *Phys. Rev. Applied*, Vol. 11, 2019, p. 054077. <https://doi.org/10.1103/PhysRevApplied.11.054077>.
- [28] Iemma, U., and Palma, G., “Optimization of metasurfaces for the design of noise trapping metadevices,” *Proceedings of the 26th International Congress on Sound and Vibration, ICSV 2019*, Canadian Acoustical Association, 411 Confederation Pkwy, Vaughan, Ontario L4K, CA, 2019, pp. 1312–1319.
- [29] Palma, G., and Burghignoli, L., “On the integration of acoustic phase-gradient metasurfaces in aeronautics,” *International Journal of Aeroacoustics*, Vol. 19, No. 6-8, 2020, pp. 294–309. <https://doi.org/10.1177/1475472X20954404>, URL <https://doi.org/10.1177/1475472X20954404>.
- [30] Palma, G., Burghignoli, L., Centracchio, F., and Iemma, U., “Innovative Acoustic Treatments of Nacelle Intakes Based on Optimised Metamaterials,” *Aerospace*, Vol. 8, No. 10, 2021. <https://doi.org/10.3390/aerospace8100296>, URL <https://www.mdpi.com/2226-4310/8/10/296>.
- [31] Palma, G., Centracchio, F., and Burghignoli, L., “Optimized metamaterials for enhanced noise shielding of innovative aircraft configurations,” *Proceedings of the 27th International Congress on Sound and Vibration, ICSV 2021*, Silesian University Press, ul. Akademicka 2A, 44-100 Gliwice, Poland, 2021, pp. 2893–2901.
- [32] Ding, Y., Statharas, E. C., Yao, K., and Hong, M., “A broadband acoustic metamaterial with impedance matching layer of gradient index,” *Applied Physics Letters*, Vol. 110, No. 24, 2017, p. 241903. <https://doi.org/10.1063/1.4986472>, URL <https://doi.org/10.1063/1.4986472>.
- [33] Wang, W., Xie, Y., Popa, B.-I., and Cummer, S. A., “Subwavelength diffractive acoustics and wavefront manipulation with a reflective acoustic metasurface,” *Journal of Applied Physics*, Vol. 120, No. 19, 2016, p. 195103. <https://doi.org/10.1063/1.4967738>, URL <https://doi.org/10.1063/1.4967738>.
- [34] Dubois, M., Shi, C., Wang, Y., and Zhang, X., “A thin and conformal metasurface for illusion acoustics of rapidly changing profiles,” *Applied Physics Letters*, Vol. 110, No. 15, 2017, p. 151902. <https://doi.org/10.1063/1.4979978>, URL <https://doi.org/10.1063/1.4979978>.

- [35] Ge, Y., Sun, H.-x., Yuan, S.-q., and Lai, Y., “Broadband unidirectional and omnidirectional bidirectional acoustic insulation through an open window structure with a metasurface of ultrathin hooklike meta-atoms,” *Applied Physics Letters*, Vol. 112, No. 24, 2018, p. 243502. <https://doi.org/10.1063/1.5025812>, URL <https://doi.org/10.1063/1.5025812>.
- [36] Ghaffarivardavagh, R., Nikolajczyk, J., Glynn Holt, R., Anderson, S., and Zhang, X., “Horn-like space-coiling metamaterials toward simultaneous phase and amplitude modulation,” *Nature Communications*, Vol. 9, No. 1, 2018, p. 1349. <https://doi.org/10.1038/s41467-018-03839-z>.
- [37] Tian, Y., Wei, Q., Cheng, Y., Xu, Z., and Liu, X., “Broadband manipulation of acoustic wavefronts by pentamode metasurface,” *Applied Physics Letters*, Vol. 107, No. 22, 2015, p. 221906. <https://doi.org/https://doi.org/10.1063/1.4936762>.
- [38] Zhu, Y.-F., Zou, X.-Y., Li, R.-Q., Jiang, X., Tu, J., Liang, B., and Cheng, J.-C., “Dispersionless manipulation of reflected acoustic wavefront by subwavelength corrugated surface,” *Scientific reports*, Vol. 5, 2015, p. 10966. <https://doi.org/https://doi.org/10.1038/srep10966>.
- [39] Wu, X., Xia, X., Tian, J., Liu, Z., and Wen, W., “Broadband reflective metasurface for focusing underwater ultrasonic waves with linearly tunable focal length,” *Applied Physics Letters*, Vol. 108, No. 16, 2016, p. 163502. <https://doi.org/https://doi.org/10.1063/1.4947437>.
- [40] Wang, X., Mao, D., and Li, Y., “Broadband acoustic skin cloak based on spiral metasurfaces,” *Scientific reports*, Vol. 7, No. 1, 2017, p. 11604. <https://doi.org/https://doi.org/10.1038/s41598-017-11846-1>.
- [41] Esfahlani, H., Karkar, S., Lissek, H., and Mosig, J. R., “Acoustic carpet cloak based on an ultrathin metasurface,” *Phys. Rev. B*, Vol. 94, 2016, p. 014302. <https://doi.org/10.1103/PhysRevB.94.014302>, URL <https://link.aps.org/doi/10.1103/PhysRevB.94.014302>.
- [42] Yu, N., Genevet, P., Kats, M. A., Aieta, F., Tetienne, J.-P., Capasso, F., and Gaburro, Z., “Light propagation with phase discontinuities: generalized laws of reflection and refraction,” *science*, 2011, p. 1210713.
- [43] Kennedy, J., and Eberhart, R., “Particle swarm optimization (PSO),” *Proc. IEEE International Conference on Neural Networks, Perth, Australia*, edited by I. of Electrical and E. Engineers, 1995, pp. 1942–1948. <https://doi.org/10.1109/ICNN.1995.488968>.
- [44] Campana, E. F., Liuzzi, G., Lucidi, S., Peri, D., Piccialli, V., and Pinto, A., “New global optimization methods for ship design problems,” *Optimization and Engineering*, Vol. 10, No. 4, 2009, p. 533.
- [45] Campana, E. F., Diez, M., Fasano, G., and Peri, D., “Initial Particles Position for PSO, in Bound Constrained Optimization,” *Advances in Swarm Intelligence*, edited by Y. Tan, Y. Shi, and H. Mo, Springer Berlin Heidelberg, Berlin, Heidelberg, 2013, pp. 112–119.
- [46] Serani, A., Diez, M., Leotardi, C., Peri, D., Fasano, G., Iemma, U., and Campana, E. F., “On the use of synchronous and asynchronous single-objective deterministic particle swarm optimization in ship design problems,” *OPT-i 2014 1st International Conference on Engineering and Applied Sciences Optimization*, edited by M. P. M.G. Karlaftis, N.D. Lagaros, 2014, pp. 1218–1240.

- [47] Pellegrini, R., Serani, A., Leotardi, C., Iemma, U., Campana, E., and Diez, M., “Formulation and parameter selection in multi-objective deterministic particle swarm for simulation-based optimization.” *Applied Soft Computing*, Vol. 58, 2007, pp. 714–731.
- [48] Iemma, U., Burghignoli, L., Centracchio, F., and Galluzzi, V., “Multi-objective optimization of takeoff and landing procedures: level abatement vs quality improvement of aircraft noise.” *43rd International Congress on Noise Control Engineering*, The Australian Acoustical Society, PO Box 1843, Toowong DC QLD 4066, AUSTRALIA, 2014, pp. 2925–2933.
- [49] Palma, G., and Iemma, U., “A metacontinuum model for phase gradient metasurfaces,” *Scientific Reports*, Vol. 13, No. 1, 2023, p. 13038. <https://doi.org/10.1038/s41598-023-39956-z>, URL <https://doi.org/10.1038/s41598-023-39956-z>.
- [50] Pierce, A. D., *Acoustics – An Introduction to its physical principles and applications*, Springer Nature Switzerland AG, Gewerbestrasse 11, 6330 Cham, Switzerland, 2019. <https://doi.org/10.1007/978-3-030-11214-1>.

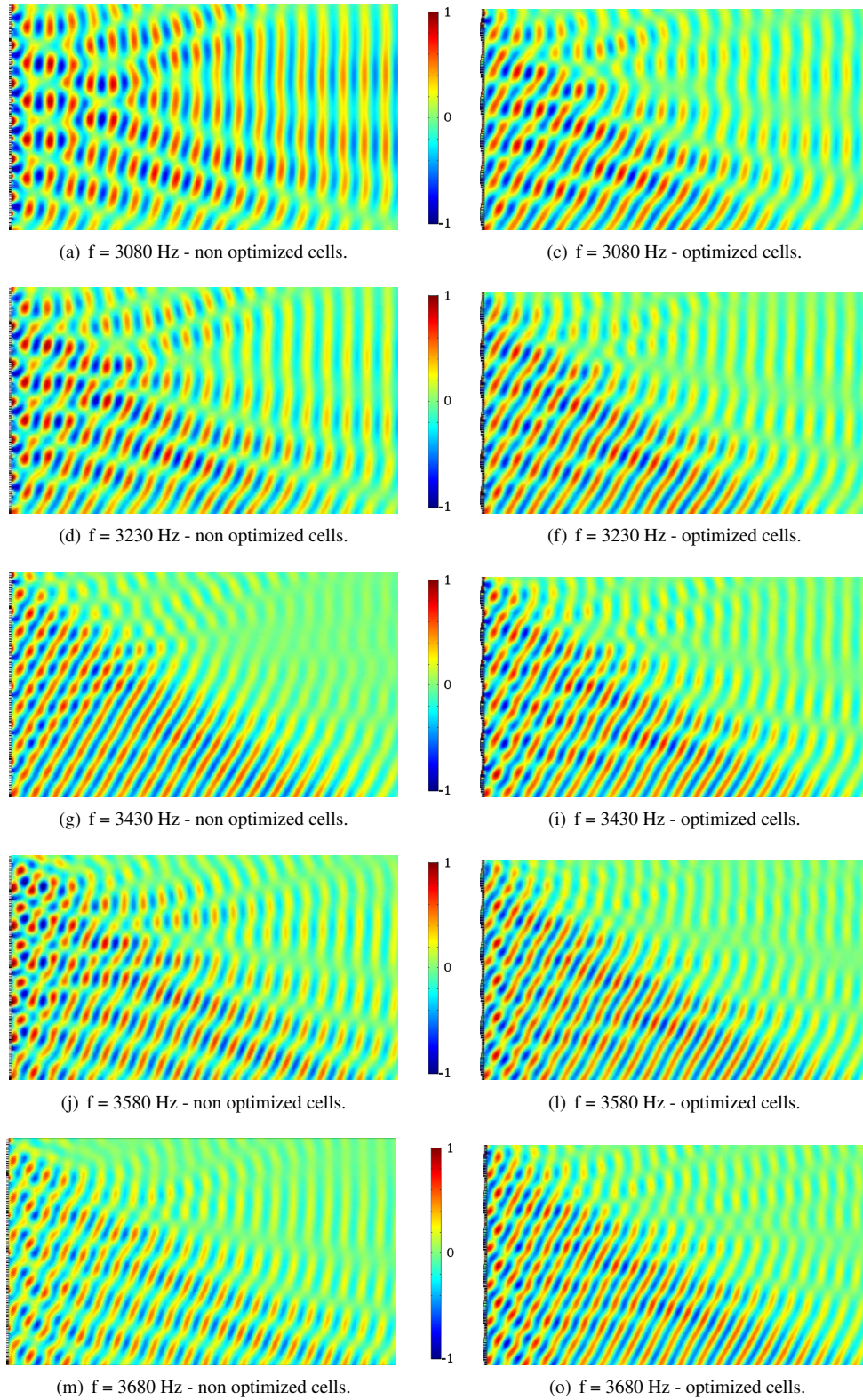


Fig. 10 Normalized scattering pressure field (real part) of reference and optimized metasurfaces from 3080 to 3680 Hz (design frequency $f_0 = 3430$ Hz), normalized by its maximum value in the domain hosting the metasurface.

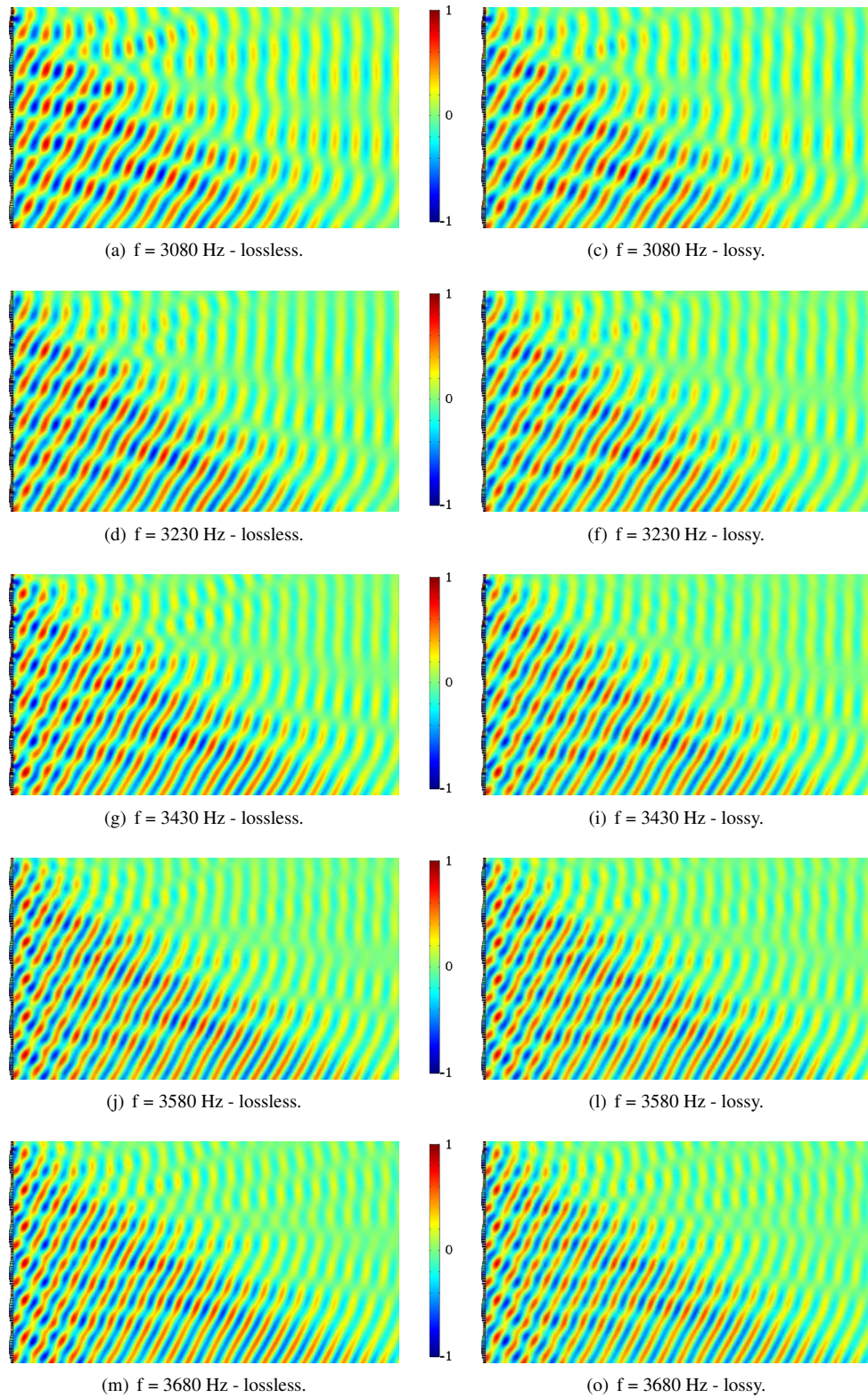


Fig. 11 Normalized scattering pressure field (real part) of the metasurface with optimized cells, obtained by lossless simulations and including visco-thermal losses in the analysis, from 3080 to 3680 Hz (design frequency $f_0 = 3430$ Hz), normalized by its maximum value in the domain hosting the metasurface.

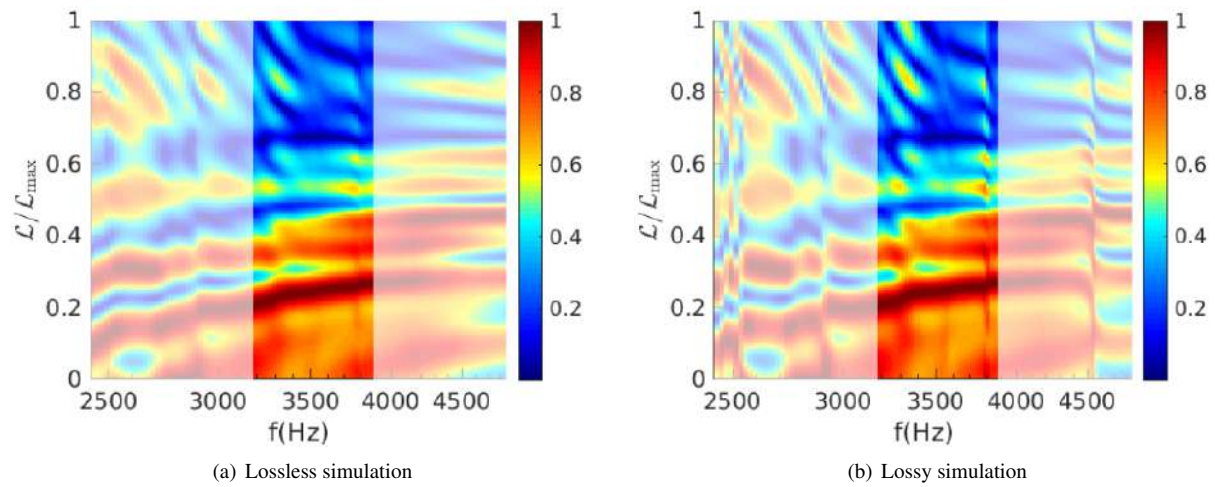


Fig. 12 Absolute value of the reflected acoustic pressure field divided by its maximum at line \mathcal{L} distant $\zeta_{\mathcal{L}} = 10\lambda_0$ from the metasurface interface, lossless simulation in (a) and including visco-thermal losses in (b).